Journal of Power Sources 294 (2015) 386–392

Contents lists available at ScienceDirect

Journal of Power Sources

journal homepage: www.elsevier.com/locate/jpowsour

Enhanced electrochemical performance of a crosslinked polyaniline-coated graphene oxide-sulfur composite for rechargeable lithium–sulfur batteries

San Moon, Young Hwa Jung, Do Kyung Kim*

Department of Materials Science and Engineering, KAIST, Daejeon 305-701, Republic of Korea

HIGHLIGHTS

- A uniform crosslinked PANI layer is fabricated on graphene oxide-sulfur composite.
- The PANI layer is synthesized by the layer-by layer assembly technique with a heating.
- The PANI layer plays a role as preventing the dissolution of polysulfides.
- A crosslinking process shows superior electrochemical performance with a high sulfur contents.

ARTICLE INFO

Article history:
Received 23 February 2015
Received in revised form
11 May 2015
Accepted 2 June 2015
Available online xxx

Keywords:
Sulfur
Battery
Conductive polymer
Crosslinking

ABSTRACT

Due to the extraordinarily high theoretical capacity of sulfur (1675 mAh g^{-1}), the lithium–sulfur (Li–S) battery has been considered a promising candidate for future high-energy battery applications. Li–S batteries, however, have suffered from limited cycle lives, mainly due to the formation of soluble polysulfides, which prevent the practical application of this attractive technology. The encapsulation of sulfur with various conductive materials has addressed this issue to some extent. Nevertheless, most approaches still present partial encapsulation of sulfur and moreover require a large quantity of conductive material (typically, >30 wt%), making the use of sulfur less desirable from the viewpoint of capacity. Here, we address these chronic issues of Li–S cells by developing a graphene oxide-sulfur composite with a thin crosslinked polyaniline (PANI) layer. Graphene oxide nanosheets with large surface area, high conductivity and a uniform conductive PANI layer, which are synthesized by a layer-by-layer method, have a synergetic interaction with a large portion of the sulfur in the active material. Furthermore, a simple crosslinking process efficiently prevents polysulfide dissolution, resulting in unprecedented electrochemical performance, even with a high sulfur content (~75%): a high capacity retention of ~80% is observed, in addition to 97.53% of the average Coulombic efficiency being retained after 500 cycles. The performance we demonstrate represents an advance in the field of lithium–sulfur batteries for applications such as power tools.

© 2015 Elsevier B.V. All rights reserved.

1. Introduction

As mobile devices deeply penetrate into our everyday lives, the demand for high-energy rechargeable batteries is rapidly increasing [1–6]. Moreover, the utilization of rechargeable batteries has broadened their use to larger applications, such as electric vehicles and electrical grid systems, which require much higher energy density. The current lithium-ion batteries (LIBs), however, which are based on traditional insertion oxide cathode materials (e.g., $LiCoO_2$, $LiMnO_4$ and $LiFePO_4$) with limited capacities approximately 100–200 mAh g^{-1}, cannot fulfill the energy demands of new devices with high power because of their heavy weight and single–electron reaction [7,8]. Therefore, considerable attention has been devoted to alternative rechargeable battery systems with significantly improved energy densities. Among various candidates, the lithium–sulfur (Li–S) battery is a promising energy system with a high theoretical energy density (2500 Wh kg^{-1}), which is approximately seven times larger than

* Corresponding author.
E-mail address: dkkim@kaist.ac.kr (D.K. Kim).

http://dx.doi.org/10.1016/j.jpowsour.2015.06.011
0378-7753/© 2015 Elsevier B.V. All rights reserved.

those of the current LIBs (~387 Wh kg^{-1}), and it utilizes the unparalleled theoretical capacity of sulfur (1675 mAh g^{-1}) that results from the fact that sulfur is a light-weight element with a two-electron reaction. As a cathode material, sulfur also has other advantages, such as nontoxicity, low cost and abundance of raw materials [9,10].

Despite the promise of sulfur, several challenges remained unsolved, such as the insulating nature of sulfur (conductivity ~10^{-30} S cm^{-1}), its large volume expansion by up to 80% upon full lithiation and its severe capacity fading during cycling [11–13]. Sulfur, unlike insertion-based electrodes, undergoes a series of structural and morphological changes during cycling, including the formation of high-order lithium polysulfides (Li_2Sn, $2 < n \leq 8$) and low-order lithium polysulfides (Li_2S_2 and Li_2S), which are insulators. Additionally, the high-order lithium polysulfides are soluble in the currently employed liquid electrolyte at the early stage of discharge. The dissolution of high-order polysulfides results in so-called shuttling effects: the dissolved polysulfides diffuse to the Li anode and are reduced, and then they diffuse back to the sulfur cathode. During this repeated round-trip of polysulfides, the active material is successively consumed, and the Li metal-electrolyte interface becomes unstable; both of these phenomena play critical roles in the severe capacity decay [14–17]. Therefore, these problems should be addressed to enable the utilization of lithium–sulfur batteries in practical applications.

One of the most popular approaches to resolve these issues has been the encapsulation of sulfur in an electrically conducting matrix, which enhances the electrical conductivity of the cathode and prevents the dissolution of high-order polysulfides [18,19]. In this regard, various mesoporous carbon materials have been studied because they are expected to be effective at trapping high-order polysulfides due to their small pore diameters. Nevertheless, this type of cathode design does not completely prevent the dissolution of polysulfides because sulfur atoms remain at the surface of the mesoporous carbon, which results in shuttling effects. Several reports successfully solved this problem, but the sulfur contents in the electrode materials were too low, resulting in a loss of energy density in the battery. A thin, conductive coating that has a high conductivity and good compatibility with sulfur minimizes the decrease in sulfur loading in the active material and is a good candidate for encapsulating sulfur. We previously reported an encapsulated sulfur electrode that adopts a sulfur nanowire array with a thin carbon coating, formed by using anodic aluminum oxide (AAO) templates [20]. The complete encapsulation of sulfur, as well as the uncommon crystal structure of monoclinic phase resulting from the unique processing, demonstrated excellent electrochemical performance despite the high sulfur content. However, it is still necessary to overcome the complex processes and the limited electrode area. To address these issues, we report here a graphene oxide-sulfur composite with a high sulfur content, which is encapsulated by the conductive polymer PANI. Diverse polymer coatings have been employed in previous studies [21–24], but standard polymer coatings have not been reported to show a noticeable ability to prevent polysulfide dissolution or maximize the effect of the polymer.

In the present investigation, we fabricate a graphene oxide-sulfur composite with a crosslinked conductive polymer (polyaniline). The formation of the crosslinked-polymer shell in the GO_S@PANI composites enhanced the cycling stability, which improved the trapping of polysulfides and played a role in creating buffer layers against the volume changes of sulfur. This approach could improve the overall electrochemical performance by resolving the aforementioned issues of lithium–sulfur batteries.

2. Experimental

2.1. Chemical and materials

Polyethyleneimine (PEI, Mw 50–100 kDa), poly(allylamine hydrochloride) (PAH) (Mw 70 kDa), poly(styrenesulfonate sodium salt) (PSS) (Mw 70 kDa), glutaraldehyde (GA) aniline monomer and sulfur were purchased from Sigma–Aldrich. All chemical reagents were used without further purification.

2.2. Preparation of graphene oxide and sulfur composite (GO-S)

Graphene oxide (GO) was prepared using a modified Hummers method, as previously reported [25]. After washing and exfoliating the GO, the centrifuged GO was freeze-dried under vacuum for two days. The graphene oxide (GO) and sulfur (weight ratio of 1:3) were mixed by ball-milling. The mixture was heated at 155 °C for 12 h in a closed vessel for sulfur infiltration.

2.3. Assembly of crosslinked PANI layer on the surface of composites

Graphene oxide-sulfur composites (GO-S) were separately dispersed in a PEI solution (1 mg/ml in 0.5 M NaCl) and allowed to adsorb for 30 min. Then, excess polyelectrolyte was removed by centrifugation and triplicate washing with 0.5 M NaCl. Subsequently, the above suspensions were alternately dispersed in PAH and PSS solutions (2 mg/ml in 0.5 M NaCl) for another 30 min, followed by triplicate washing in 0.5 M NaCl. After the assembly of a desired number of PAH/PSS layers, the coated particles were dispersed in a 5% glutaraldehyde (GA) aqueous solution for 30 min. Finally, these sample suspensions were incubated at 70 °C for 20 min. The prepared aqueous dispersion of polymer-coated sulfur particles was added into the aniline monomer solution mixed with 1 M hydrochloric acid (HCl) under stirring. After 30 min, the equivalent number of moles (with respect to aniline) of a 22.8 wt% aqueous ammonium persulfate (APS) solution was slowly added, followed by oxidative polymerization at 0 °C. The reaction duration was 24 h. The resultant green solid, GO-S@PANI, was obtained by centrifugation and washed with water and ethanol thoroughly to remove excess ions and monomers. The final product was dried under vacuum at ambient temperature for 24 h. To crosslink the PANI layer, GO-S@PANI was heated at 180 °C for 1 h in air.

2.4. Characterization

The weight fractions of carbon and sulfur were determined by an elemental analyzer (Flash 2000, Thermo Scientific). The morphology of the materials was observed using field-emission scanning electron microscopy (SEM, Hitachi S-4800) and field-emission transmission electron microscopy (TEM, Tecnai G^2 F30 S-Twin). Elemental mapping was performed using energy dispersive spectroscopy (EDS, Tecnai G^2 F30 S-Twin) to visualize the location of each element. X-ray diffraction (XRD) data were recorded on a diffractometer (Model D/MAM 2500, Rigaku, Co.), using Cu Kα radiation ($\lambda = 1.5406$ Å at 40 kV and 300 mA), and it was collected over a 2θ range of 10°–70°.

2.5. Cell assembly and battery testing

To prepare working electrodes, the synthesized material was mixed with the conducting carbon Super P (Timcal) and the binder sodium alginate (Sigma Aldrich) in a weight ratio of 75:15:10, with DI water as a dispersant, to make a viscous slurry that was cast onto aluminum foil and dried at 60 °C under vacuum for 24 h. Electrochemical measurements were performed by preparing 2032-type

coin cells (MTI Corporation) that were assembled in an argon-filled glovebox. The prepared sample and lithium foil (Alfa Aesar) were used as the working and counter/reference electrodes, respectively. The electrolyte was prepared by dissolving 1 M lithium bis(trifluoromethanesulfonyl)imide (LiTFSI) in cosolvents of 1,3-dioxolane (anhydrous, contains ~75 ppm BHT as an inhibitor, 99.8%, Sigma–Aldrich) and 1,2-dimethoxyethane (anhydrous, 99.5%, Sigma–Aldrich) (volume ratio = 1:1). Before the electrolyte preparation, these solvents were stored over molecular sieves for 24 h to remove moisture. Polypropylene membranes (Celgard, Inc.) were used as separators. Galvanostatic measurements were performed in the potential range of 1.0–3.0 V vs. Li/Li^+ using a battery cycler (WBS3000, Wonatech). Electrochemical impedance spectroscopy (EIS) at open-circuit voltages was measured using a potentiostat (VMP3, Biologic) from 1 MHz to 10 mHz under AC stimuli with 10 mV of amplitude. The C-rates for all coin cells are calculated based on the theoretical capacity of sulfur, for which 1C is 1675 mA g^{-1}. All of the electrochemical measurements were performed at 25 °C.

3. Results and discussions

Key concepts in the electrode design are a graphene oxide-sulfur (GO-S) composite and conductive polymer layers with minimal wall thickness. As schematically summarized in Fig. 1, GO nanosheets were first synthesized by a modified Hummers method (Fig. 1a) [25]. The GO and sulfur were heated for sulfur infiltration into the gaps between the GO nanosheets. Then, the sulfur-infiltrated GO were coated by PANI (polyaniline) and cured to crosslink the PANI layers. Detailed procedures are described in the experimental section. Each step in the procedure could have a great impact on the final cell performance, and the following points are especially noteworthy.

Above all, the PANI coating procedure is most critical because it defines the uniformity and thickness of the coating layers. For improved electrochemical performance of lithium–sulfur batteries, the development of appropriate composite active materials is imperative. Although the sulfur located between the gaps of graphene oxide nanosheets is electrically reactive and can reduce the shuttling effects, the sulfur on the surface of graphene oxide nanosheets can directly contact the electrolyte, which results in polysulfide dissolution. Fig. S1 shows the cycle performances of graphene oxide-sulfur composites with various sulfur contents. The composite with 31% sulfur was synthesized by heating the composite with 91% sulfur. Excess sulfur atoms, which were exposed on the surface of the GO nanosheets, were removed by further heating at 300 °C for 2 h in Ar. As expected, the composite with 31% S presented good cyclability compared with the composite with 91% S because it prevented the shuttling effect due to the presence of fewer exposed sulfur. However, despite the good cyclability of a composite with a low sulfur loading, this material is unsuitable for high-performance applications because of the small quantity of active material, which results in lower energy density of the battery. This drawback can be overcome by utilizing GO-S composites with a thin, conducting PANI layer. In this case, we coated the PANI layer onto GO-S composites using the layer-by-layer technique, as previously reported [26,27]. The positively charged poly(allylamine hydrochloride) (PAH) and negatively charged poly(-styrenesulfonate sodium salt) (PSS) were alternatively adsorbed onto the surface of the graphene oxide-sulfur particles by electrostatic interaction and induced uniform PANI coating layers. Additionally, the layer thickness could be controlled by regulating the number of adsorption layers, which react as a catalyst for the polymerization of aniline.

Moreover, crosslinking a polymer by heating can decrease the permeability of the layers as a result of the rearrangement of the polymer chains into a preferred structure [26,28–31]. This arrangement procedure is accompanied by increased electrical conductivity, elastic modulus and condensation of the polymer, resulting in a reduction in the pore size. It can be anticipated that the crosslinked-polymer layers increase the electron and lithium ion diffusion and the elasticity for volume expansion, but they are nearly impermeable for polysulfides. Therefore, the aforementioned problems of lithium–sulfur batteries can be solved by crosslinked conductive polymer layers.

Fig. 2a show scanning electron microscopy (SEM) images of stacked graphene oxide-sulfur composite. Fig. 2b–d presents surface images of the materials during each synthetic step. As

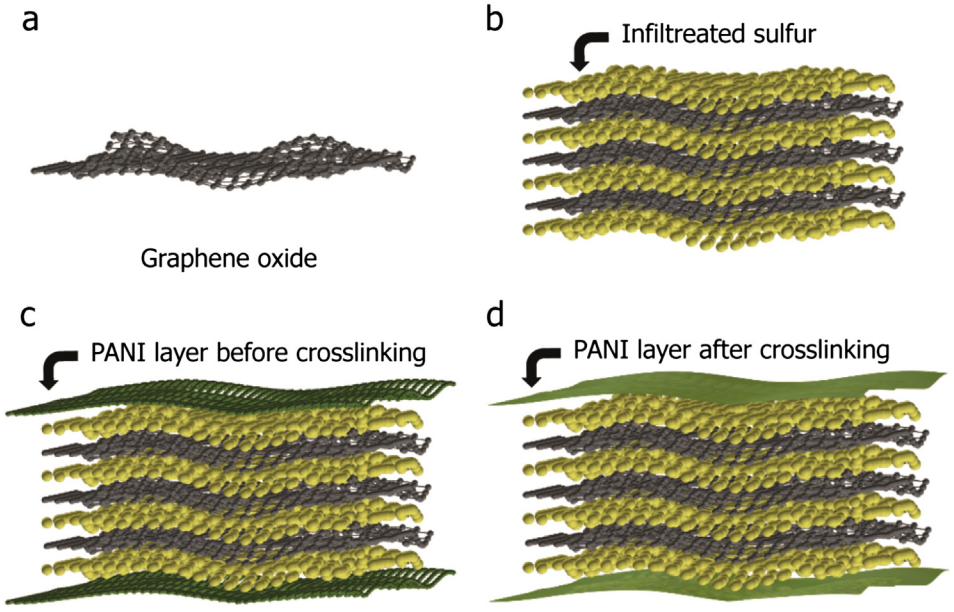

Fig. 1. Schematic illustration of synthesis procedure of the GO-S@PANI. a) Graphene oxide nanosheets, b) Sulfur-infiltrated graphene oxide nanosheets, c) PANI coated GO and sulfur composite and d) GO-S@PANI after crosslinking. The composite annealed at 180 °C for 1 h in air.

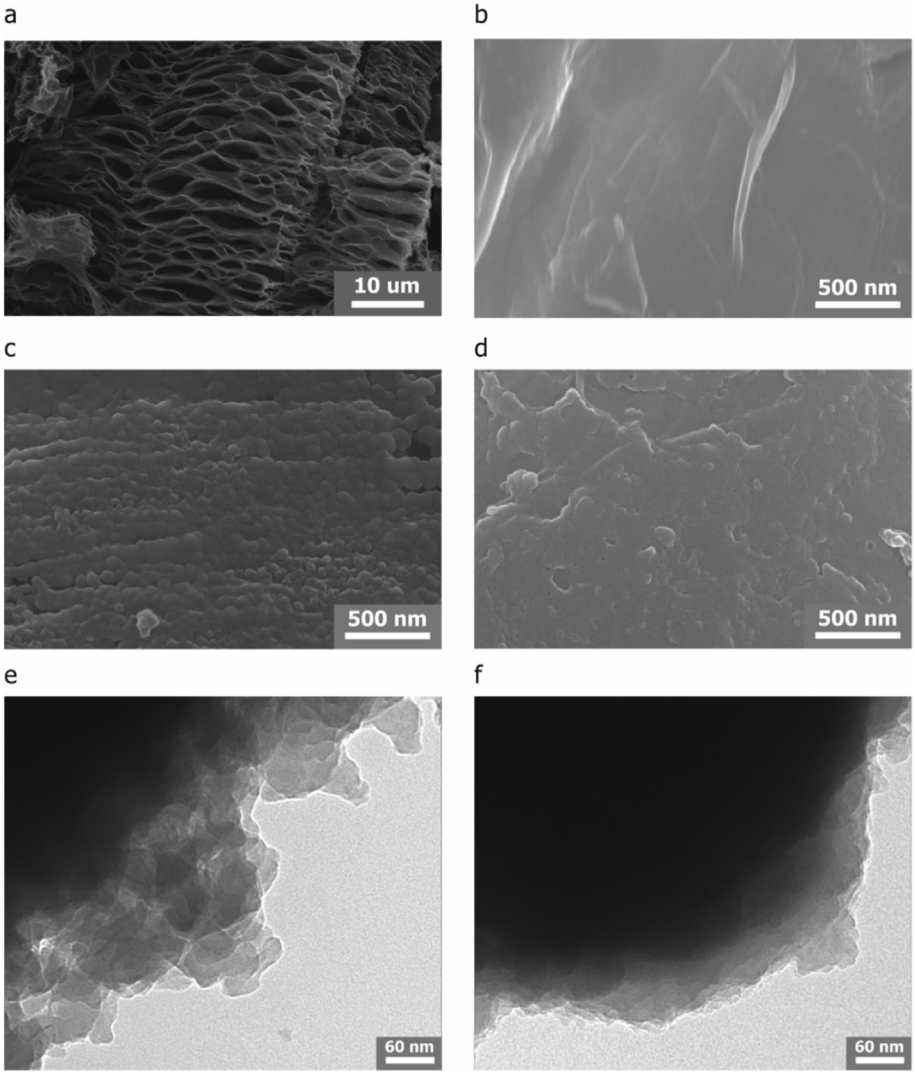

Fig. 2. Morphology characterizations of graphene oxide and graphene oxide-sulfur composites. a) SEM image of sulfur-infiltrated graphene oxides (GO-S), b) their surface, c) PANI coated GO-S (GO-S@PANI) and d) GO-S@PANI after curing at 180 °C. e) TEM image of the GO-S@PANI and f) GO-S@PANI after curing.

displayed in 2b, the surface morphologies GO-S appear indicates uniform mixing of the sulfur with GO. Fig. 2c and d shows the images of PANI-coated GO-S composites (S: 75%) before and after curing at 180 °C, respectively. It can be seen that the morphology is completely different. Whereas as-prepared GO-S composites with PANI layers show agglomerated particles (Fig. 2c), the cured composites show denser surface structures (Fig. 2d). The surface morphologies were characterized further (Fig. 2e and f) by high-resolution transmission electron microscopy (HRTEM). The HRTEM images indicate that the cured surfaces have fewer pores and a sufficiently dense coating layer to prevent polysulfide dissolution.

The FT-IR spectra of the particles shows the characteristic peaks of PANI-coated particles and cured PANI, as shown in Fig. 3a. The spectrum of prepared-PANI and PANI-coated GO-S (GO-S@PANI) showed the characteristic peaks at approximately 1580 cm^{-1} for the C═N stretching mode of the quinonoid rings, 1500 cm^{-1} for C═C stretching mode of benzenoid rings and 1300 cm^{-1} for the C–N stretching mode. The vibrational bands at approximately 1140 and 827 cm^{-1} are attributed to the aromatic ring in-plane and out-of-plane C–H bending [32,33]. The peaks in the FT-IR spectra of the cured-PANI composites were noticeably suppressed upon annealing. The bands at approximately 1580 and 1500 cm^{-1} were slightly shifted in the IR adsorption of the cured samples. The quinone rings in the cured sample were opened, and its band becomes located at 1600 cm^{-1} and shorter compared with the benzenoid band at 1510 cm^{-1}. In addition, the vibrational bands between 1400 and 1100 cm^{-1} merged into a single peak to give a broad band after annealing. The disappearance of the peak at 1300 cm^{-1} can be assigned to a C–H stretching vibration with aromatic conjugation, indicating the crosslinking of PANI [34]. In general, the peak-intensity ratio of the quinoid-to-benzenoid peak (quinoid/benzenoid) has been utilized to evaluate the chemical changes in a PANI sample upon thermal treatment [35]. After curing, the ratio of quinoid to benzenoid decreased, which indicates conversion of the quinoid rings into benzenoid rings, as illustrated in the inset of Fig. 3a. The FT-IR results indicate that the polymer layers are successfully crosslinked after the curing process.

To verify the structural characteristics of the nanocomposites, X-ray diffraction (XRD) was conducted on pure sulfur powder, GO, GO-S and GO-S@PANI before and after curing, as shown in Fig. 3b. The XRD patterns of the GO-S and GO-S@PANI nanocomposites reveal the orthorhombic sulfur peaks with reduced intensity due to the graphene oxide and amorphous PANI. It is also shown that the

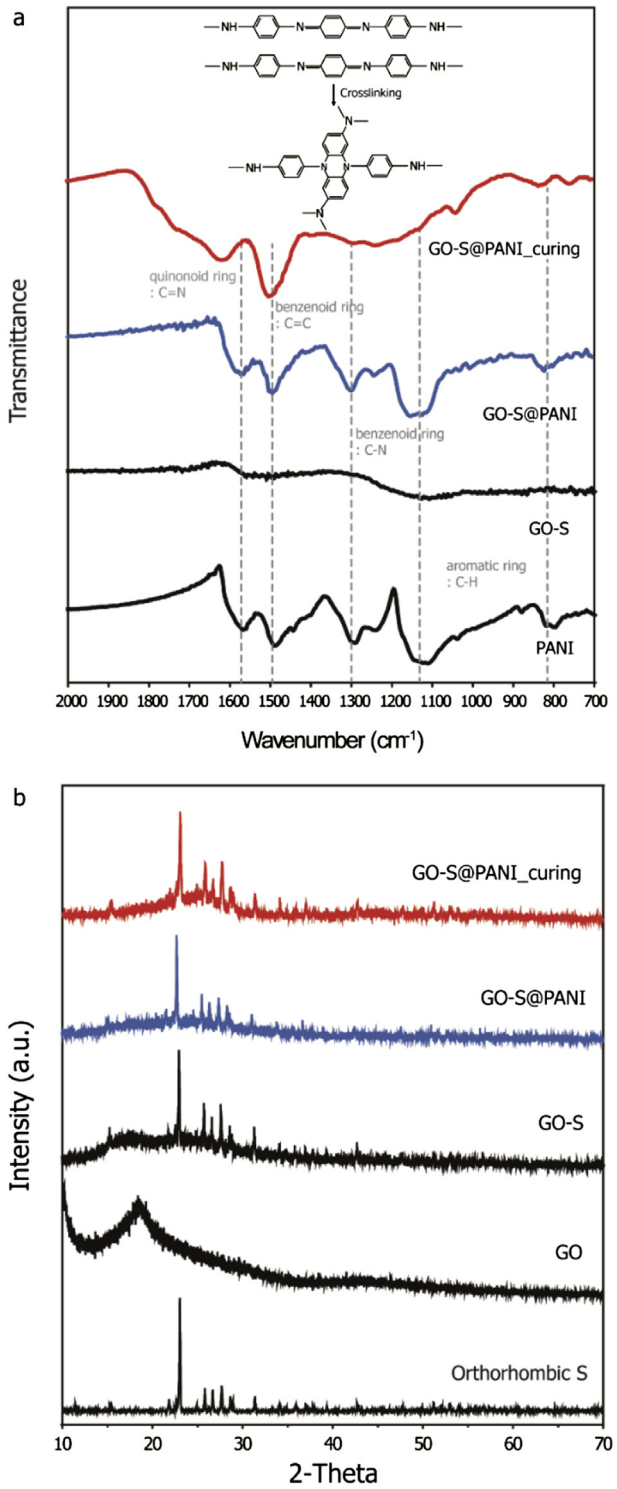

Fig. 3. (a) FTIR spectrum of PANI and composites. (b) XRD patterns of pristine sulfur and composites after each procedure.

XRD patterns of the crosslinked samples correspond to the orthorhombic sulfur peaks.

The electrochemical performance of the GO-S@PANI was evaluated by measuring coin-type half-cells. A solution of 1 M lithium bis(trifluoromethanesulfonyl)imide (LiTFSI) dissolved in the co-solvent of 1,3-dioxolane and 1,2-dimethoxyethane (volume ratio = 1:1) was used as an electrolyte. Detailed cell-preparation and measurement conditions were described in the experimental section. Although the GO-S@PANI shows much higher discharge capacity (~1050 mAh g^{-1}) than the GO-S composite (~850 mAh g^{-1}), problems such as incomplete coating and the lower conductivity of the PANI layers on the GO-S surface, resulting in a low Coulombic efficiency and capacity retention, still remain. The crosslinking of the PANI layers by curing may be a solution to address these problems, as will be discussed.

Fig. 4a shows the tenth discharge–charge profiles of Li-sulfur cells made of each composite cathode during 0.5C cycling. The GO-S composite with crosslinked PANI layers results in the lowest overcharge during the charge reaction with a higher discharge capacity. It was found that there were two plateaus at approximately 2.3 and 2.0 V in each case as for typical sulfur electrodes, due to the two-step reduction of sulfur in the presence of Li ions [36,37]. Interestingly, the plateaus occurred at lower voltage for the PANI-coated composites, implying a relatively high-potential polarization after PANI coating. The reason for the high-potential polarization was investigated by EIS. It can be observed from the typical Nyquist plots (Fig. 4b) that each impedance spectrum has two distinctive parts composed of a semicircular arc in the high-frequency region and a straight line in the middle-to-low-frequency region. The high-frequency region corresponds to the charge-transfer resistance (R_{ct}) caused by the electrochemical reactions at the contact interface between the electrode and electrolyte solution [38]. The R_{ct} values obtained from the semicircular arc diameters were 40.06, 67.45 and 52.21 Ω for GO-S, GO-S@PANI and cured GO-S@PANI, respectively. It is notable that the PANI-coated samples exhibit higher R_{ct} values (67.45 and 52.21 Ω) than the uncoated sample (40.06 Ω). This indicates that the PANI coating layer hindered the charge transfer compared with highly conductive graphene oxide. Nevertheless, the curing procedure reduces the R_{ct}, suggesting better charge transfer at the electrode/electrolyte interface by changing the surfaces of the PANI-coated GO-S composites. Additionally, the lines in the middle-to-low-frequency region in the PANI-coated samples display steeper increases (Warburg diffusion behavior) than that of the uncoated one, which is representative of faster ion diffusion in the electrode materials [39]. Hence, the higher capacity with lower overcharge for a cured GO-S@PANI sample is attributed to the crosslinked PANI coating that enhances the ion diffusion, in addition to the prevention of polysulfide dissolution by the cured surface structure.

Fig. 4c and d shows the cycling performance, which is the most critical aspect in Li–S cell operation, tested in the galvanostatic mode. For this testing, the capacities were measured at 0.5 and 1C, respectively. As displayed in Fig. 4c, the bare GO-S electrode presented poor cyclability with continuously lower Coulombic efficiencies. Whereas the bare GO-S electrode delivers an initial discharge capacity of 1101 mAh g^{-1}, the capacity retains only 469 mAh g^{-1} (48.0% retention with respect to the capacity in the second cycle) after 100 cycles at a rate of 0.5C. The average Coulombic efficiency in the cycle range from 2 to 100 was low at ca. 68.1%. In the case of PANI coating, the GO-S@PANI delivers a higher discharge capacity of 1246 mAh g^{-1} in the second cycle at a current rate of 0.5C with a capacity retention of 61.4%, and the average Coulombic efficiency was 76.8%, which presented slightly better performance than the GO-S composite due to the conductive polymer coating, as previously reported [23,24]. However, interestingly, the cured, crosslinked GO-S@PANI sample exhibits striking performance enhancements in both cyclability and Coulombic efficiency. After crosslinking the GO-S@PANI electrode, 80.6% (with regard to 1248 mAh g^{-1} of discharge capacity in the second cycle) of capacity retention was achieved after 100 cycles, and further, an excellent Coulombic efficiency of 98.7% was also attained at 0.5C cycling. To confirm the longer cyclability of the cured sample, the cycling performance of the GO-S@PANI_curing electrode at the 1C

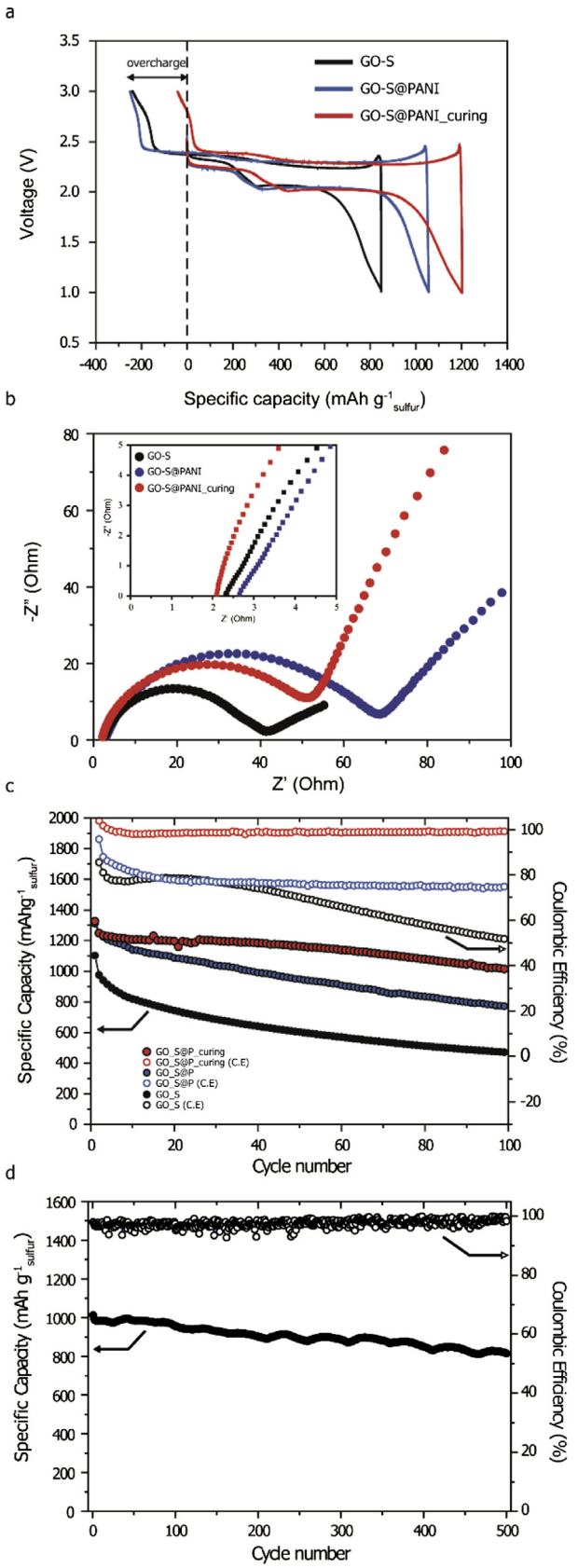

Fig. 4. Electrochemical performance of sulfur cathode. (a) Galvanostatic curves of the composites in 10th cycle at C-rate of 0.5C (1C = 1675 mAh g^{-1}), (b) EIS of the cathodes, (c) Capacity retentions and Coulombic efficiencies of the composites at discharge rates of 0.5C and (d) Cyclability of the GO-S@PANI_curing. The same measurement but with a charge and discharge rate of 1C.

rate was tested by an additional 500 cycles. A high capacity retention of 80.43% as well as 97.53% of the average Coulombic efficiency were obtained, again demonstrating the superior performance of the cured sample. There are two possible reasons for the high performance of the cured GO-S@PANI electrode.

First, the crosslinked PANI layer coating can prevent the dissolution of polysulfides so that more high-order polysulfides could be converted into Li_2S without loss due to dissolution. This is supported by the fact that the major difference in capacity comes from the voltage plateaus at 2.3 V (Fig. 4a). The cured GO-S@PANI electrode displays a much higher capacity at 2.3 V (~420 mAh g^{-1}) than those of GO-S and GO-S@PANI (~300 mAh g^{-1}). It is speculated that the amount of the freshly formed long-chain polysulfide dissolution decreases due to encapsulation by the crosslinked PANI layers. To verify the results of the high capacity retention and Coulombic efficiency of the cured GO-S@PANI electrode, simple beaker cell tests were performed with each electrode. Fig. 5a shows the typical setup of the beaker cell with a sulfur electrode as the cathode and Li metal as the anode in an Ar-filled glovebox. Fig. 5b presents a comparison of the color changes in the electrolytes of the GO-S, GO-S@PANI and cured GO-S@PANI electrode after 50 cycles at 1C and the electrolyte before electrochemical testing. It can be inferred that the GO-S and GO-S@PANI could not suppress the dissolution of high-order polysulfides, based on the observation that the electrolytes changed from colorless to yellow after 50 cycles. The color of the electrolytes in the GO-S electrode without the PANI coating turned a deeper yellow than that of the GO-S@PANI electrode. Furthermore, almost no changes were observed compared with initial electrolytes for the electrolytes in the cured GO-S@PANI electrode, even after 50 cycles, further supporting that the crosslinked PANI layer can successfully suppress the dissolution of polysulfides.

Second, the other possible reason is that the higher electronic conductivity of a crosslinked PANI layer as a conductive coating compared with that of bare PANI is capable of enhancing the electrochemical performance of insulating materials. The EIS spectra in Fig. 4b show that R_{ct} decreases from 67.45 Ω (GO-S@PANI) to 52.21 Ω (GO-S@PANI/curing) after curing, which indicates that the conducting PANI shell facilitates electrical conduction. The equivalent series resistance (R_s) can be observed from the x-intercept in the inset of Fig. 4b, which includes the ionic resistance of the electrolytes, intrinsic resistance of the active material and contact resistance at the active material/current collector interface [38,40]. The GO-S, GO-S@PANI and cured GO-S@PANI electrodes delivered R_s values of 2.29, 2.65 and 2.09 Ω, respectively. This also can be related to the improved electrochemical capacitive behavior of the crosslinked PANI layer, which can be ascribed to the higher conductivity and charge-transfer capability of the crosslinked PANI layer.

4. Conclusions

In summary, a uniform crosslinked polyaniline layer, synthesized by the layer-by-layer assembly technique in combination with a heat treatment is successfully fabricated on graphene oxide-sulfur composites. The composite is investigated as an electrode material for lithium–sulfur batteries. The crosslinked PANI layer avoids the chronic issues previously reported in lithium–sulfur batteries. In particular, the crosslinked PANI layer plays an important role as an electrolyte-blocking layer, preventing the dissolution of polysulfides. This effect induces the stable cycling capacity of the cured GO-S/PANI composites. The strategy employed in this work to produce a uniform crosslinked PANI layer is also applicable to other electrode materials in lithium–sulfur batteries to develop stable electrode materials that avoid the shuttling effect.

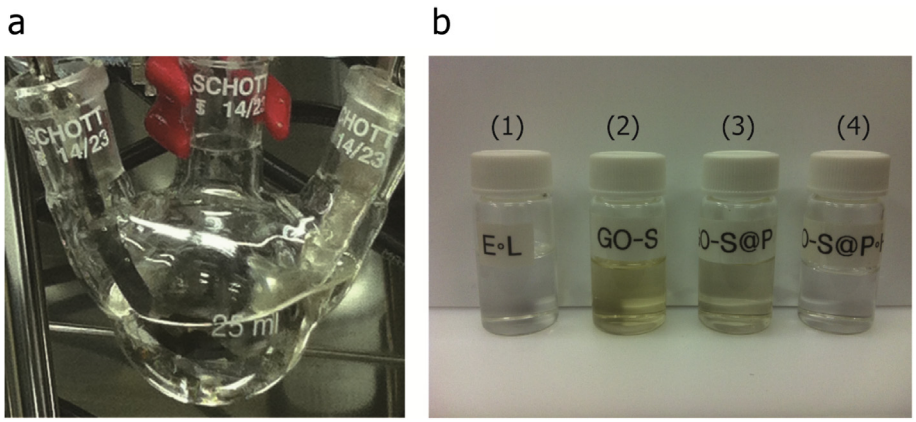

Fig. 5. Polysulfide dissolution test of the prepared sulfur electrode. (a) Beaker cell test, (b) (1) the electrolyte before electrochemical testing, the electrolytes of the (2) GO-S, (3) GO-S@PANI and (4) cured GO-S@PANI electrode after 50 cycles at 1C.

Acknowledgments

Authors gratefully acknowledge financial support from the EEWS Research Project of the KAIST EEWS Research Center (Grant No. N01150034). This research was also supported by the Program to Solve Climate Changes (NRF-2010-C1AAA001-2010-0029031) of Korea (NRF) funded by the Ministry of Science, ICT & Future Planning.

Appendix A. Supplementary data

Supplementary data related to this article can be found at http://dx.doi.org/10.1016/j.jpowsour.2015.06.011.

References

[1] M. Armand, J.M. Tarascon, Nature 451 (2008) 652–657.
[2] J.B. Goodenough, Y. Kim, Chem. Mater. 22 (2010) 587–603.
[3] B. Scrosati, J. Hassoun, Y.K. Sun, Energy Environ. Sci. 4 (2011) 3287–3295.
[4] P.G. Bruce, S.A. Freunberger, L.J. Hardwick, J.M. Tarascon, Nat. Mater. 11 (2012) 19–29.
[5] M.S. Whittingham, Chem. Rev. 104 (2004) 4271–4301.
[6] C. Liu, F. Li, L.P. Ma, H.M. Cheng, Adv. Mater. 22 (2010) E28–E62.
[7] S.Y. Chung, J.T. Bloking, Y.M. Chiang, Nat. Mater. 1 (2002) 123–128.
[8] A. Manthiram, J. Phy. Chem. Lett. 2 (2011) 176–184.
[9] N. Jayaprakash, J. Shen, S.S. Moganty, A. Corona, L.A. Archer, Angew. Chem. Int. Ed. 50 (2011) 5904–5908.
[10] X.L. Ji, L.F. Nazar, J. Mater. Chem. 20 (2010) 9821–9826.
[11] C.D. Liang, N.J. Dudney, J.Y. Howe, Chem. Mater. 21 (2009) 4724–4730.
[12] F. Wu, J.Z. Chen, R.J. Chen, S.X. Wu, L. Li, S. Chen, T. Zhao, J. Phys. Chem. C 115 (2011) 6057–6063.
[13] Y.Z. Fu, A. Manthiram, RSC Adv. 2 (2012) 5927–5929.
[14] H. Yamin, A. Gorenshtein, J. Penciner, Y. Sternberg, E. Peled, J. Electro. Soc. 135 (1988) 1045–1048.
[15] D. Aurbach, E. Pollak, R. Elazari, G. Salitra, C.S. Kelley, J. Affinito, J. Electro. Soc. 156 (2009) A694–A702.
[16] C. Barchasz, F. Mesguich, J. Dijon, J.C. Lepretre, S. Patoux, F. Alloin, J. Power Sources 211 (2012) 19–26.
[17] L.M. Suo, Y.S. Hu, H. Li, M. Armand, L.Q. Chen, Nat. Comm. 4 (2013).
[18] X.L. Ji, K.T. Lee, L.F. Nazar, Nat. Mater. 8 (2009) 500–506.
[19] G.Y. Zheng, Y. Yang, J.J. Cha, S.S. Hong, Y. Cui, Nano Lett. 11 (2011) 4462–4467.
[20] S. Moon, Y.H. Jung, W.K. Jung, D.S. Jung, J.W. Choi, D.K. Kim, Adv. Mater. 25 (2013) 6547–6553.
[21] H. Li, M.Q. Sun, T. Zhang, Y.Q. Fang, G.C. Wang, J. Mater. Chem. A 2 (2014) 18345–18352.
[22] H.W. Chen, W.L. Dong, J. Ge, C.H. Wang, X.D. Wu, W. Lu, L.W. Chen, Sci. Rep. 3 (2013).
[23] G.C. Li, G.R. Li, S.H. Ye, X.P. Gao, Adv. Energy Mater. 2 (2012) 1238–1245.
[24] W.D. Zhou, Y.C. Yu, H. Chen, F.J. DiSalvo, H.D. Abruna, J. Am. Chem. Soc. 135 (2013) 16736–16743.
[25] C.H. Lim, A.G. Kannan, H.W. Lee, D.K. Kim, J. Mater. Chem. A 1 (2013) 6183–6190.
[26] L. Duan, Q. He, X.H. Yan, Y. Cui, K.W. Wang, J.B. Li, Biochem. Biophy. Res. Comm. 354 (2007) 357–362.
[27] L. Duan, J.C. Lu, W.Y. Liu, P. Huang, W.S. Wang, Z.C. Liu, Coll. Surf. A Phy. Engin. Asp. 414 (2012) 98–103.
[28] W.X. Song, Q. He, H. Mohwald, Y. Yang, J.B. Li, J. Control. Release 139 (2009) 160–166.
[29] W.J. Tong, C.Y. Gao, H. Mohwald, Chem. Mater. 17 (2005) 4610–4616.
[30] R. Mueller, K. Kohler, R. Weinkamer, G. Sukhorukov, A. Fery, Macromolecules 38 (2005) 9766–9771.
[31] K. Kohler, G.B. Sukhorukov, Adv. Funct. Mater. 17 (2007) 2053–2061.
[32] G. Sonmez, H.B. Sonmez, C.K.E. Shen, F. Wudl, Adv. Mater. 16 (2004) 1905.
[33] J.X. Huang, R.B. Kaner, Angew. Chem. Int. Ed. 43 (2004) 5817–5821.
[34] J.F. Chen, Y.T. Xu, Y.F. Zheng, L.Z. Dai, H.H. Wu, Comptes Rendus Chim. 11 (2008) 84–89.
[35] S. Palaniappan, B.H. Narayana, J. Poly. Sci. Part A Poly. Chem. 32 (1994) 2431–2436.
[36] J.C. Guo, Y.H. Xu, C.S. Wang, Nano Lett. 11 (2011) 4288–4294.
[37] S. Xin, L. Gu, N.H. Zhao, Y.X. Yin, L.J. Zhou, Y.G. Guo, L.J. Wan, J. Amer. Chem. Soc. 134 (2012) 18510–18513.
[38] Z. Gao, W.L. Yang, J. Wang, B. Wang, Z.S. Li, Q. Liu, M.L. Zhang, L.H. Liu, Energy & Fuels 27 (2013) 568–575.
[39] Z.F. Li, H.Y. Zhang, Q. Liu, L.L. Sun, L. Stanciu, J. Xie, ACS Appl. Mater. Interfaces 5 (2013) 2685–2691.
[40] H.X. Yang, T. Song, L. Liu, A. Devadoss, F. Xia, H. Han, H. Park, W. Sigmund, K. Kwon, U. Paik, J. Phy. Chem. C 17 (2013) 17376–17381.